The Effect of Disorder on Crackling Noise in Fracture Phenomena

Zoltán Halász,[1] Gábor Timár[2] and Ferenc Kun[2]

[1]*Institute of Nuclear Research, H-4001 Debrecen, P.O.Box: 51, Hungary*
[2]*Department of Theoretical Physics, University of Debrecen, H-4010 Debrecen, P.O.Box: 5, Hungary*

We study the effect of disorder on crackling noise accompanying the fracture of heterogeneous materials. Two different types of system are considered: we analyze the three-point bending of a bar shaped specimen where the boundary and loading conditions ensure that crackling occurs during the propagation of a single crack; then we study a bundle of fibers where noise emerges as a consequence of spatially uncorrelated stick-slip rearrangements. We show that bursts characterizing the jerky propagation of a crack have a power law size distribution with an exponent which does not depend on the amount of disorder. Our calculations revealed that varying the amount of disorder in a stick-slip system, a phase-transition occurs: at high disorder stick-slip rearrangements occur in small bursts, while at low disorder macroscopic avalanches snap the system. Our investigations demonstrate that the relevance of disorder on crackling noise is strongly influenced by the presence or absence of stress concentrations in the system.

§1. Introduction

The fracture of heterogeneous materials is a very important scientific problem with a broad spectrum of technological applications. During the last two decades experiments have revealed that the heterogeneous micro-structure of materials has a strong effect on fracture processes which can only be understood in the framework of statistical physics. Assuming a perfectly crystalline structure, the fracture strength σ_c of materials can be estimated as the load needed to separate two crystal planes, which implies that σ_c should fall in the order of magnitude of the Young modulus E of the material $\sigma_c \sim E$. However, measured strength values are typically 2–3 orders of magnitude smaller than the Young modulus. The reason is that heterogeneous materials contain defects, flaws, micro-cracks, which become unstable at loads much below E and trigger catastrophic failure of the system.[1)]

Besides making materials weaker, disorder has also a very important positive effect in the fracture process: growing micro-cracks can stop when reaching a material region with a higher local strength. As a consequence, the macroscopic failure of heterogeneous materials is preceded by a damage accumulation process in the form of nucleation of new micro-cracks, furthermore, of the growth and arrest of the existing ones. Nucleating and propagating cracks emit acoustic waves which can be recorded by sensitive microphones as acoustic noise. Such crackling noise measurements provide very useful information about the microscopic dynamics of progressive damaging and it can also be exploited to forecast the imminent failure event. Recently, the application of statistical physics to understand crackling noise has provided a novel insight into fracture phenomena allowing also for new technological applications.[1)] On a more general basis, crackling noise can be defined

as the jerky response of disordered systems to a slow external driving.[2)–5)] Examples of systems exhibiting crackling noise can be mentioned from the Barkhausen noise in ferromagnets,[2),5),6)] through the plastic deformation of materials,[7)] to the emergence of earthquake sequences.[4),8)] Beyond its practical relevance, it is a very interesting problem to embed the crackling noise accompanying fracture into the general framework of the statistical physics of complex systems exhibiting crackling phenomena.

To capture the effect of disorder in materials breakdown, recently several stochastic fracture models have been proposed such as the fiber bundle model (FBM)[9)–12)] and lattice models of fuses or springs.[1),13)–18)] On the basis of these models, analytic calculations and computer simulations revealed that the fracture of disordered materials shows interesting analogies with phase transitions and critical phenomena having several universal features independent of specific material details.[1),8),9),12),13)] As an alternative approach, discrete element modeling (DEM) is applied when a realistic representation of the mechanics of materials is of high importance under time dependent conditions. DEM is based on a physical discretization of a specimen whose time evolution is followed by molecular dynamics simulations.[15)–18)]

In this paper we study the emergence of crackling noise in two different types of systems: first we analyze the propagation of a single crack in a specimen subject to three-point bending, then we study noise generated in a bundle of fibers which can rearrange themselves with a stick-slip mechanism under an increasing load. The main goal of our investigations is to reveal the effect of the amount of disorder on crackling noise in the presence and absence of stress concentration. We show that under three-point bending conditions the crack proceeds and opens in bursts which have a power law size distribution. The bursts are correlated sequences of microscopic breakings which result in jumps of the crack tip. Decreasing the amount of disorder the jumps become longer, however, the exponent of the size distribution remains the same. On the basis of discrete element simulations we propose a scaling form for the burst size distribution of propagating cracks obtained at different amount of disorders.

Varying the amount of disorder in a bundle of fibers with stick-slip dynamics we show that the system undergoes a disorder driven phase transition: at high amount of disorder only small avalanches of fiber slips appear, however, at low disorder macroscopic avalanches snap the system. We demonstrate analytically that the size distribution of slip avalanches exhibits a power law behavior in both phases, however, with different values of the exponent. In the high disorder phase we determine the scaling form of the burst size distribution and obtain the value of the cutoff exponent. The analytical results are complemented by large scale Monte Carlo simulations of FBMs. The main difference between the two systems considered is that under three-point bending conditions bursts are generated by spatially correlated breakings while in the stick-slip fiber bundle local slip events do not have any spatial correlations (mean field type system). In the presence of spatial correlations the amount of disorder just controls the typical scale of the characteristic quantities of bursting events, while in the mean field system a phase transition is obtained.

§2. Crack propagation in three-point bending

Three-point bending is a standard engineering test where a bar shaped specimen is clamped at the two ends and a point load is applied in the middle perpendicular to the longer axis of the bar. Under an increasing load the bar bends and finally breaks due to a crack which appears in the middle along the load direction. This testing method is mainly used in the engineering literature to characterize the quasi-static fracture strength of structural materials such as concrete. On the other hand, three-point bending experiments provide an excellent opportunity to study the propagation of a single crack in a disordered environment which is a challenging problem for the statistical physics of fracture. Recently, it was found experimentally that the cracking of a bar under three point bending proceeds in bursts which are characterized by power law distributions.[19] In the experiments bars of ferromagnetic materials such as steel were subject to three-point loading applied dynamically by the Charpy impact machine. The impact machine is a pendulum whose arm is raised to an initial height which then hits the specimen at the bottom of its swing. As the steel bar breaks, magnetic noise is generated which is recorded in the form of an irregular voltage time series composed of a large number of peaks. The experiments showed that the amplitude, area and energy of peaks have power law distributions where the values of the exponents are sensitive to the type of fracture, i.e. the noise spectra of ductile materials are characterized by higher exponents than the brittle ones.[19] The boundary and loading conditions ensured in the experiments that the damage localizes to a relatively thin layer of the specimen giving rise to a single growing crack so that the crackling noise measured during the loading process characterizes the crack propagation.[19]

In order to obtain a deeper theoretical understanding of the experimental findings we use a discrete element modeling technique and perform realistic computer simulations of the loading process. In the following we briefly present the model construction then we analyze the dynamics of crack propagation obtained by simulations focusing on the noisy character of the process.

2.1. *Discrete element model for heterogeneous materials*

Recently, we have worked out a two-dimensional dynamical model of deformable, breakable granular solids, which enables us to perform molecular dynamics simulation of fracture and fragmentation of solids in various experimental situations.[15)–18)] Our model is an extension of those models which are used to study the behavior of granular materials applying randomly shaped convex polygons to describe grains.[17] The initial set of polygons is obtained by the Voronoi tessellation of a square from which specimens of appropriate shapes can be cut out. The average polygon size l_p sets the characteristic length scale of the model system. The polygons are considered to be rigid bodies which can overlap when pressed against each other. We introduce a repulsive force between the overlapping particles proportional to the overlap area.[15)–18)] To capture the elastic behavior of solids we connect the unbreakable, undeformable polygons (grains) by elastic beams. The beams have two important roles in the model construction: they ensure cohesion and they are able

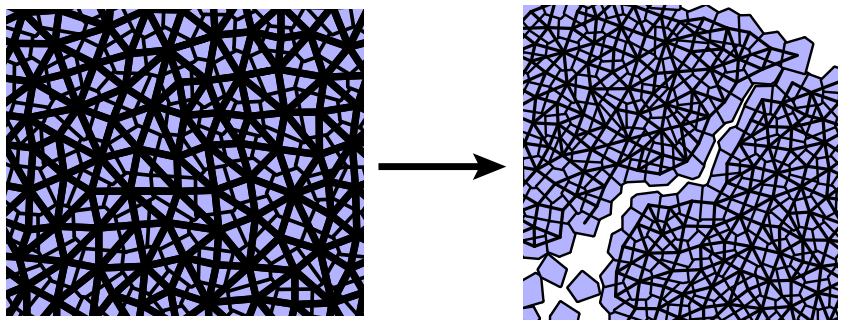

Fig. 1. (left) Neighboring polygons of the initial Voronoi tessellation are connected by beams. This way a triangular beam lattice is obtained. (right) Due to subsequent breaking of beams a crack forms along the edge of polygons.

to break which is essential to model fracture processes. The beams can be elongated, compressed, sheared and bent so that they exert forces and torques on the polygons to which they are attached. Figure 1 presents an example of the polygon structure and the beam lattice attached to the polygons.

In the simulations a bar shaped specimen is considered with an aspect ratio 1:5 corresponding to the experimental standards. In order to make a realistic representation of three-point loading, the three loading plates are realized by additional polygonal elements, i.e. squares in Fig. 2 with side length $S = 5l_p$ much smaller than the longer side $L = 1000l_p$ of the bar $S \ll L$. These loading plates interact with the particles of the bar via the overlap force, however, no beams are coupled to them. Strain controlled loading of the bar is implemented in such a way that the two loading plates at the bottom are fixed while the third one on the top is moved vertically downward in Fig. 2 with a constant speed v_0. The moving plate overlaps the boundary polygons on the top of the bar which results in an increasing loading force. The stiffness of the plates is set high enough to keep the overlap below 20% of the average polygon area. Simulations were carried out varying the value of v_0 in a range, which allows for an efficient damping of the elastic waves and ensures a reasonable CPU time for the computations. The main advantage of three-point bending tests is that the highly stressed zone where the crack appears falls in the middle of the bar which helps to make efficient monitoring of the fracture process. In order to simplify the numerical measurements on crack propagation, we introduce a "weak" line in the middle of the bar in such a way that solely those beams are allowed to break which connect the two sides of the line.

2.2. *Disordered beam breaking*

The beams, modeling cohesive forces between grains, can be broken according to a physical breaking rule, which takes into account the stretching and bending of the connections

$$\left(\frac{\varepsilon}{\varepsilon_{th}}\right)^2 + \frac{\max(|\Theta_1|, |\Theta_2|)}{\Theta_{th}} \geq 1. \qquad (2{\cdot}1)$$

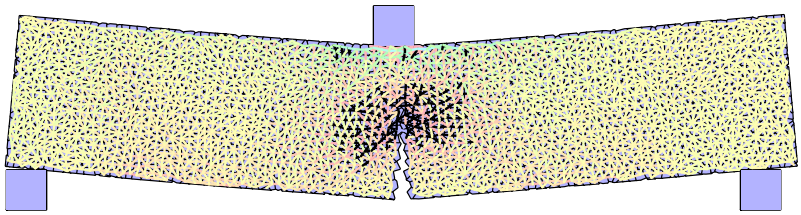

Fig. 2. (Color online) Three-point bending of a bar composed of polygonal particles. The particles are coupled by elastic beams which are colored according to the longitudinal deformation (yellow: nearly unstressed beams; red and black: elongated beams; blue and green: compressed beams). Beams are allowed to break solely along the center line of the bar. We are investigating the jerky propagation of the crack along the weak line. A relatively small sample is presented to have a clear view on the details of the model construction. The two loading plates at the bottom are fixed while the third one on the top moves downward.

Here ε denotes the longitudinal deformation of a beam, while Θ_1 and Θ_2 are bending angles at the two beam ends. The breaking rule Eq. (2·1) contains two parameters $\varepsilon_{th}, \Theta_{th}$ controlling the relative importance of the stretching and bending breaking modes, respectively. The energy stored in a beam just before breaking is released in the breakage giving rise to energy dissipation. At the broken beams along the surface of the polygons cracks are generated inside the solid and as a result of the successive beam breaking the solid falls apart (see Fig. 1). The time evolution of the polygonal solid is obtained by solving the equations of motion of the individual polygons. At each iteration step we evaluate the breaking criterion Eq. (2·1) and remove those beams which fulfill the condition. The simulation is continued until the entire system relaxes, i.e. there is no breaking of the beams during some hundreds of consecutive time steps. (For more details of the model construction see Refs. 16)–18).)

The breaking parameters ε_{th} and Θ_{th} of beams are stochastic variables in the model, i.e. they are sampled from probability density functions $p(\varepsilon_{th})$ and $p(\Theta_{th})$. The Weibull distribution provides a comprehensive description of the stochastic fracture strength of materials, hence, for both threshold values the Weibull form is prescribed

$$p_{\lambda,m}(x) = \frac{m}{\lambda}\left(\frac{x}{\lambda}\right)^{m-1} e^{-(x/\lambda)^m}, \tag{2·2}$$

where x denotes the two breaking thresholds $\varepsilon_{th}, \Theta_{th}$. The Weibull distribution has two parameters: λ sets the characteristic scale of threshold values while the exponent m determines the scatter of the variable. Increasing the value of the exponent m the width of the Weibull distribution Eq. (2·2) decreases and converges to the delta function in the limit $m \to \infty$. Computer simulations were carried out using fixed values of the scale parameters $\lambda_\varepsilon = 0.04$ and $\lambda_\Theta = 0.09$ varying the Weibull exponents in the range $1 \leq m \leq 15$ for both threshold distributions.

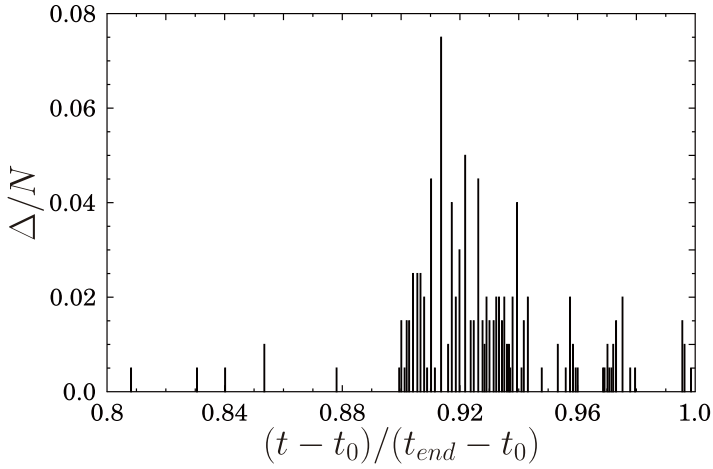

Fig. 3. Time series of bursts in a single fracture simulation. The bursts are correlated breaking sequences of beams which then result in sudden jumps of the crack tip. N denotes the total number of beams along the weak interface where the crack propagates. For all the simulations its value was set to $N = 200$. At the beginning of the loading process, for a considerable time no breaking occurs, most of the breaking events appear at larger deflections close to final breakdown. Hence, we magnify the final section of the bending process. t_0 and t_{end} denote the time of the first and the last beam breaking, respectively.

2.3. *Crackling noise during crack propagation*

A snapshot of the computer simulation of a three-point bending test is presented in Fig. 2. The color code shows that the bottom of the specimen is highly elongated that's why the crack starts here. In the vicinity of the crack tip the beams are strongly elongated indicating a high stress concentration ahead the crack which provides the driving force for crack propagation. At the top of the bar the color code indicates that compressive stresses arise. Since under compression beams do not break, the compressive zone has a stabilization effect in the sense that it ensures a gradual advancement of the crack tip.

The constant speed of the loading plate implies a strain controlled loading of the specimen at a fixed strain rate. This way of loading has the consequence that in each iteration step of the molecular dynamics simulation either no beam breaking occurs or only a single beam breaks. After a local breaking event the stress gets redistributed increasing the stress concentration on the intact elements ahead the crack. The load redistribution may give rise to additional breakings resulting in a correlated trail of breaking events. In order to identify bursts of local breakings we introduce a correlation time t_{corr}: if the time difference of two consecutive beam breakings occurring at times t_i and t_{i+1} is smaller than the correlation time $t_{i+1} - t_i < t_{corr}$ the two breakings are considered to belong to the same burst. The value of the correlation time was chosen in such a way that it is larger than the time step Δt used in the integration of the equation of motion but it is much smaller than the total duration T of crack propagation, i.e. we set $t_{corr} = 10\Delta t$ for which $10^5 t_{corr} < T$ holds. The size of bursts Δ is defined as the number of beams breaking during the

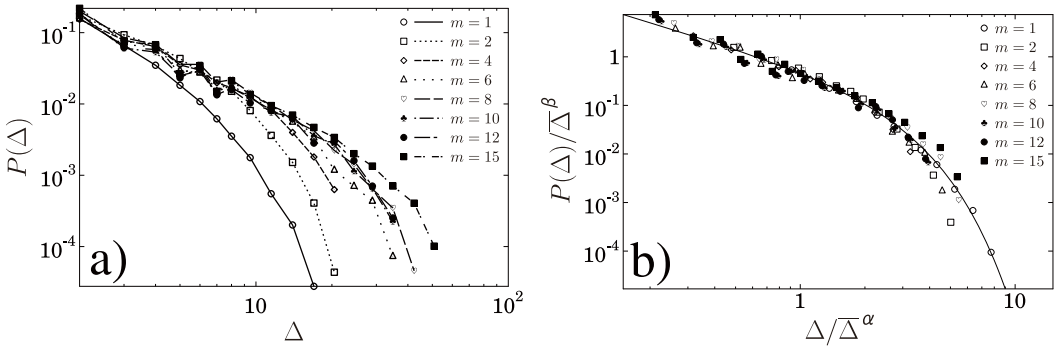

Fig. 4. (a) Burst size distributions obtained at different values of the Weibull exponent m. Increasing m, i.e. decreasing the amount of disorder in the model, burst sizes Δ span a broader interval. For small bursts a power law functional form is obtained while for large bursts the distribution decays rapidly. (b) Scaling plot of the burst size distributions. Rescaling along both axis with an appropriate power of the average burst size $\overline{\Delta}$ a nice data collapse is obtained.

correlated sequence.

Figure 3 presents the size of bursts in a single fracture simulation at the time of their appearance. Since these breaking events are spatially correlated the bursts can be considered as sudden jumps of the crack tip. It can be seen in the figure that the bursts are separated by silent periods with variable length. These waiting times between bursts characterize the duration of states where the crack tip is pinned due to the presence of some strong beams. At the beginning of the loading process the bursts are small compared to the cross section of the specimen (maximum crack length), however, with increasing deflection of the bar the burst size Δ increases and reaches a maximum somewhat before the last breaking. After the maximum the burst size decreases showing that as the crack approaches the top of the bar it slows down due to the compressive zone.

We determined numerically the size distribution of bursts $P(\Delta)$ varying the amount of disorder in the failure thresholds. The size distribution obtained at different values of the Weibull exponent is presented in Fig. 4(a). It is interesting to note that increasing the Weibull exponent m, i.e. decreasing the amount of disorder, the bursts get larger but the functional form does not change. For small bursts a power law behavior is obtained followed by a rapidly decreasing cutoff regime. Figure 4(b) demonstrates that using the average burst size $\overline{\Delta}$ as a scaling variable, the burst size distributions obtained at different m values can be collapsed on a master curve. The data collapse implies the scaling structure

$$P(\Delta) = \overline{\Delta}^{\beta} g(\Delta/\overline{\Delta}^{\alpha}), \tag{2·3}$$

where the values of the exponents were determined numerically $\alpha = 1.6 \pm 0.05$ and $\beta = 2.1 \pm 0.07$ which provide the best quality collapse. The exponent of the power law regime of the distribution $P(\Delta) \sim \Delta^{-\tau}$ was obtained as $\tau = 1.31 \pm 0.04$.

The results demonstrate that the growth of crack is not a smooth process, the slow driving results in a jerky crack propagation which is composed of a large number

of discrete steps. The growth steps are sudden outbreaks with a variable length. The correlation of consecutive local breakings leads to a power law functional form. The most interesting outcome of the calculations is that the amount of disorder only affects the characteristic scale of bursts but the functional form and the value of the exponent remain the same. Comparing the value of the exponent τ to recent experimental results on three-point bending fracture of ferromagnetic materials[19] a reasonable agreement is obtained.

§3. Stick-slip avalanches in a fiber bundle model

Another limiting case of fracture phenomena where crackling noise arises is the spatially uncorrelated cracking of an extended system. In order to compare the effect of disorder on the crackling noise for spatially correlated and uncorrelated breaking events, now we consider a mean field model of fracture, i.e. a fiber bundle model (FBM) where fibers can undergo subsequent rearrangements with stick-slip mechanism before they break. In our model over-stressed fibers do not break, instead they increase their relaxed length in a slip event until they can sustain the load. The system is driven by small load increments giving rise to the slip of a single fiber which may then trigger an entire avalanche of slip events due to load redistribution in the bundle. Assuming an infinite range of interaction, we analyze the size distribution of slip avalanches varying the amount of threshold disorder in the system.

3.1. *Fiber bundle with stick-slip dynamics*

Our model consists of N fibers assembled in parallel. Under an increasing external load σ the fibers exhibit a linearly elastic behavior characterized by the same Young modulus E. In the model when the deformation ε of a fiber reaches a threshold value ε_{th} the fiber does not break, instead, its relaxed length increases until the load reduces to zero on the fiber. The mechanism of relaxation is the slip of the fiber end, or it can also be interpreted as the unfolding of subunits of fibers which provide some stored length.[20] The slip thresholds ε_{th}^i, $i = 1, \ldots, N$ are random variables with a probability density $p(\varepsilon_{th})$ and distribution function $P(\varepsilon_{th})$.

After the slip event the fiber gets sticked again so that it can support load

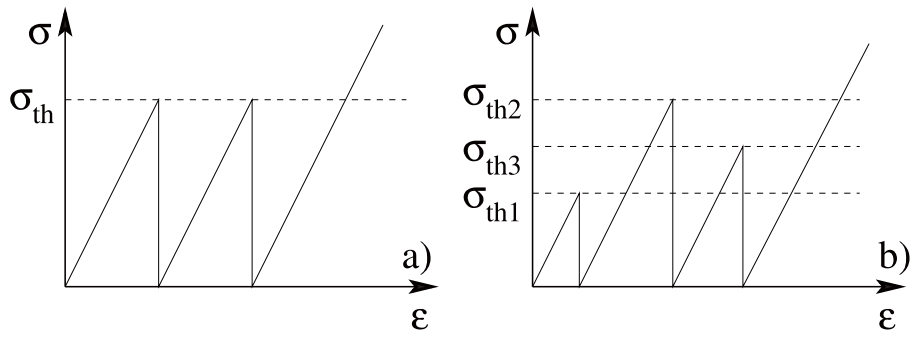

Fig. 5. Constitutive behavior of single fibers for quenched (a) and annealed slip thresholds (b). The young modulus E remains the same during the sequence of stick-slip events.

and can suffer further slips. The load kept by fiber i at a deformation ε after slipping reads as $\sigma_i = E(\varepsilon - \varepsilon_{th}^i)$ so that no hardening or softening is assumed in the system. When a fiber slips again either the same slip threshold is retained (quenched disorder) or new threshold values can be drawn from the same probability distribution $p(\varepsilon_{th})$ (annealed disorder). The total number of slip events k_{max} a fiber can suffer is a very important parameter of the model which can vary in the range $1 \leq k_{max} < +\infty$. For the load redistribution following slip events we assume an infinite range of interaction, i.e. equal load sharing, which is ensured by the condition that the strain ε is the same for all fibers. The present analysis is restricted to the case of quenched disorder so that the load of fiber i in the bundle after $k_i \leq k_{max}$ slips takes the form $\sigma_i = E(\varepsilon - k_i\varepsilon_{th}^i)$. The constitutive behavior of single fibers is presented in Fig. 5. Further details of the model construction can be found in Ref. 20). We note that our model can also be conceived as the fiber bundle analogue of the Burridge-Knopoff model of earthquakes.[21)]

On the basis of the assumption of equal load sharing the constitutive equation $\sigma(\varepsilon)$ of the parallel bundle can be obtained analytically by integrating the load kept by subsets of fibers with slip index $0 \leq k \leq k_{max}$, where $k = 0$ means intact fibers[20)]

$$\sigma(\varepsilon) = E\varepsilon\left[1 - P(E\varepsilon)\right] + \sum_{k=1}^{k_{max}-1} \int_{\varepsilon/(k+1)}^{\varepsilon/k} p(E\varepsilon_1)E\left(\varepsilon - k\varepsilon_1\right) d\varepsilon_1 + \int_0^{\varepsilon/k_{max}} p(E\varepsilon_1)E\left(\varepsilon - k_{max}\varepsilon_1\right) d\varepsilon_1. \quad (3{\cdot}1)$$

The above integrals have to be performed over the entire loading history of the bundle. For very large deformations $\varepsilon \to \infty$, practically all fibers have suffered k_{max} slips so that Eq. (3·1) can be rewritten as $\sigma(\varepsilon) \sim E\varepsilon - k_{max}E\int_0^{\varepsilon/k_{max}} p(\varepsilon_1)\varepsilon_1 d\varepsilon_1$ where the integral provides the average value of the slip thresholds $\langle\varepsilon_{th}\rangle$. This shows that the bundle has an asymptotic linear behavior with the initial value of the Young modulus, however, when unloading the system $\sigma \to 0$ an irreversible permanent deformation remains with a maximum ε_r^{max} proportional to the average slip length $\langle\varepsilon_{th}\rangle$ and to the number of slip events k_{max} allowed $\varepsilon_r^{max} = k_{max}\langle\varepsilon_{th}\rangle$.

In the model calculations Weibull distribution of the form of Eq. (2·2) was applied for the failure thresholds to be able to easily control the amount of disorder similarly to the case of three-point bending. In all the calculations of the stick-slip FBM the scale parameter of threshold values was fixed $\lambda = 1$, while the Weibull exponent was varied in the range $1 \leq m < 50$. The constitutive curve of the model is presented in Fig. 6(a) for several values of the maximum allowed slips k_{max} setting the Weibull exponent to $m = 1$. It can be seen that as k_{max} increases the asymptotic linear regime is preceded by a longer and longer plateau which indicates an apparent plastic response.

3.2. *Slip avalanches*

We investigate the response of the stick-slip bundle to a slowly increasing external load. Quasi-static stress controlled loading of the fiber bundle can be performed by incrementing the external load with a small amount $\delta\sigma$ just to provoke the slip

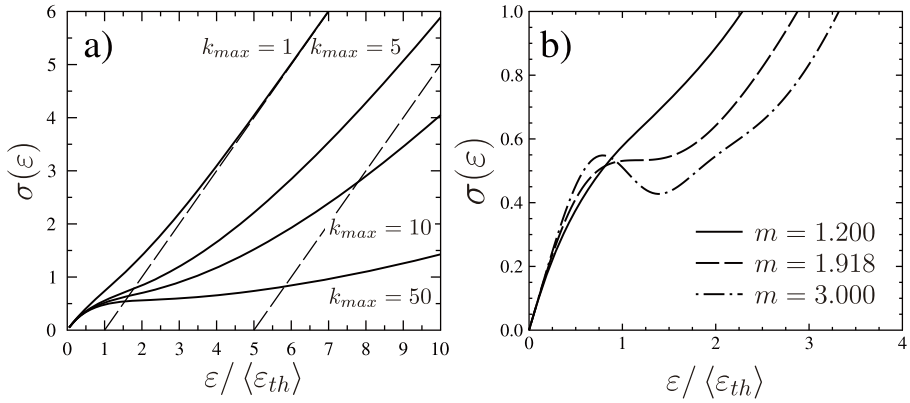

Fig. 6. Constitutive behavior of the bundle (a) for $m = 1$ (exponential distribution) varying the value of the maximum number of allowed failures k_{max}, while (b) demonstrates $\sigma(\varepsilon)$ for $k_{max} = 3$ varying the value of m. For the exponential distribution $\sigma(\varepsilon)$ is monotonically increasing for all k_{max}. However, varying the value of m in the range $1 < m$ at a fixed $1 < k_{max}$ the constitutive curve changes from strictly monotonous to a shape where local maxima and minima appear. The transition between the two regimes appears at $m_3^c \approx 1.918$.

of a single fiber. The external load σ is kept constant during the slip, hence, the load dropped by the slipping fiber must be overtaken by the other ones which can give rise to further slip events. This way a single slip induced externally can trigger an entire avalanche of slips, which increases the macroscopic strain ε of the system by the amount $\delta\varepsilon$. This jerky microscopic dynamics has the consequence that the deformation of the bundle has a step-wise increase under a quasi-statically increasing external load σ similarly to the jerky extension of the growing crack under three-point bending. The size of slip avalanches Δ is defined as the number of fibers slipping in the avalanche and the microscopic response of the bundle is characterized by the probability distribution of burst sizes $P(\Delta)$.

For simple fiber bundles where fibers break irreversibly when the local load surpasses their threshold value, it has recently been shown[9),10)] for the case of equal load sharing that the size distribution of avalanches $P(\Delta)$ can be obtained in a closed analytical form as

$$P(\Delta) \approx \frac{e^{\Delta}}{\sqrt{2\pi}\Delta^{3/2}} \int_0^{\varepsilon_c} p(\varepsilon) \frac{1-a(\varepsilon)}{a(\varepsilon)} e^{\Delta[a(\varepsilon)-\ln a(\varepsilon)]} d\varepsilon. \qquad (3{\cdot}2)$$

In the above expression, $a(\varepsilon)$ denotes the average number of fibers which break as a consequence of a single fiber failure induced by the external load increment at the deformation ε. The integration over ε is carried out up to the critical point ε_c of the system where catastrophic collapse occurs. The dominating contribution to the integral is provided by the vicinity of the maximum of the exponent of the integrand $\psi(\varepsilon) = a(\varepsilon) - \ln a(\varepsilon)$, which is obtained at $a = 1$. It can be shown analytically that the distribution has a power law decay $P(\Delta) \sim \Delta^{-\tau}$. The exponent $\tau = 5/2$ proved to be universal for a broad class of disorder distributions where the macroscopic constitutive curve $\sigma(\varepsilon)$ of the system has a single quadratic maximum.[9)–11)]

In order to understand the dynamics of slip avalanches first the sequence of slipping events has to be analyzed. We can determine the probability density $p_k^{k+1}(\varepsilon)$ of events that a fiber which has suffered k slips until the deformation ε was reached, will slip again due to the strain increment $d\varepsilon$

$$p_k^{k+1}(\varepsilon) = \frac{1}{k+1} p\left(\frac{\varepsilon}{k+1}\right), \quad 0 \leq k < k_{max}, \tag{3·3}$$

where p is the original probability density of the slip thresholds. Keeping the load σ fixed during the slip, the arising strain increment reads as $\delta\varepsilon_k = \varepsilon_{th}^i / N = \varepsilon/(kN)$. It follows that the average number of fibers $a(\varepsilon)$ which slip as a consequence of a single slip can be determined as $a(\varepsilon) = N \sum_{k=0}^{k_{max}-1} \delta\varepsilon_k p_k^{k+1}(\varepsilon)$ which leads to the form

$$a(\varepsilon) = \varepsilon \sum_{k=1}^{k_{max}} \frac{1}{k^2} p\left(\frac{E\varepsilon}{k}\right). \tag{3·4}$$

For the analysis of the burst size distributions it is useful to express the derivative of the constitutive equation $\sigma(\varepsilon)$ of Eq. (3·1) in terms of $a(\varepsilon)$

$$\frac{d\sigma}{d\varepsilon} = E\left[1 - \sum_{k=1}^{k_{max}} \frac{\varepsilon}{k^2} p\left(\frac{E\varepsilon}{k}\right)\right] = E\left[1 - a(\varepsilon)\right], \tag{3·5}$$

which show that the constitutive curve $\sigma(\varepsilon)$ has extrema at locations ε_c where the average number of induced slips becomes unity $a(\varepsilon_c) = 1$, furthermore, at the extremal points of $a(\varepsilon)$ the constitutive curve $\sigma(\varepsilon)$ has an inflexion point $d^2\sigma/d\varepsilon^2 = 0$.

3.3. *Disorder induced phase transition*

In the following we analyze the statistics of slip avalanches varying the amount of disorder m and the maximum number of allowed slips k_{max}. Using Eqs. (3·1), (3·4) and (3·5) we can determine analytically the phase diagram of the system on the $m - k_{max}$ plane which classifies all possible functional forms of the constitutive curves $\sigma(\varepsilon)$ and of avalanche size distributions $P(\Delta)$. For this purpose we write the average number of induced slips $a(\varepsilon)$ in the form $a(\varepsilon) = \sum_{k=1}^{k_{max}} a_k(\varepsilon)$, where each term $a_k(\varepsilon) = (\varepsilon/k^2) p(E\varepsilon/k)$ has a single maximum at the strain ε_k^c. It can be shown analytically that if a_1 has a maximum at ε_1^c with the value a_1^c, then the maxima of the other terms $a_k(\varepsilon)$ are placed equidistantly as $\varepsilon_k^c = k\varepsilon_1^c$ with decreasing values $a_k^c = a_1^c/k$. Since the functions $a_k(\varepsilon)$ overlap each other, the consecutive maxima of $a(\varepsilon)$ do not coincide with that of $a_k(\varepsilon)$, however, the equidistant spacing and the decreasing sequence remains valid. Substituting the Weibull distribution the above analysis results in $\varepsilon_k^c = k\lambda$ and $a_k^c = m/(ke)$, where e is the base of natural logarithm. It can be seen that for $k_{max} = 1$, when only a single slip is allowed, at the critical Weibull exponent $m_1^c = e$ the constitutive curve $\sigma(\varepsilon)$ has an inflexion point at the position ε_1^c where $a(\varepsilon)$ has a maximum with the value $a(\varepsilon_1^c) = 1$. It can be shown similarly that for any $k_{max} \geq 1$ one can find an $m_{k_{max}}^c$ value of the Weibull exponent, where the constitutive curve has an inflexion point with the properties $d\sigma/d\varepsilon|\varepsilon_{k_{max}}^c = 0$ and $d^2\sigma/d\varepsilon^2|\varepsilon_{k_{max}}^c = 0$, where at the same time $a(\varepsilon_{k_{max}}^c) = 1$ and $da/d\varepsilon|\varepsilon_{k_{max}}^c = 0$ hold.

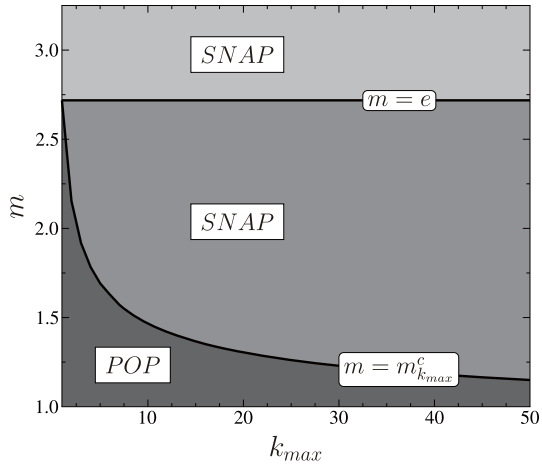

Fig. 7. Phase diagram of the system. The decreasing line indicates the $m^c_{k_{max}}$ curve which separates the POP and $SNAP$ regimes. Above the $m = e$ line the constitutive curve has a maximum already at $k_{max} = 1$.

Figure 7 presents the phase diagram of the system where the decreasing line represents the $m^c_{k_{max}}$ curve which was determined numerically. For $k_{max} = 1$ the critical Weibull exponent is $m^c_1 = e$ and $m^c_{k_{max}} \to 1$ holds for $k_{max} \to +\infty$. In order to obtain the asymptotics of the size distribution of slip avalanches $P(\Delta)$ analytically from Eq. (3·2) for parameters along the $m^c_{k_{max}}$ curve, the Taylor expansion of $a(\varepsilon)$ and $\psi(\varepsilon)$ about $\varepsilon^c_{k_{max}}$ has to be continued up to the first non-vanishing terms, which result in a power law asymptotics $P(\Delta) \sim \Delta^{-\tau}$ with the exponent $\tau = 9/4$. The parameter regime of m and k_{max} below the $m^c_{k_{max}}$ curve of Fig. 7 defines the high disorder phase of the model, where $\sigma(\varepsilon)$ is monotonically increasing $d\sigma/d\varepsilon > 0$ and the maximum of $a(\varepsilon)$ is always smaller than 1. Figures 6(a) and (b) illustrate the constitutive behavior $\sigma(\varepsilon)$ of the model varying k_{max} and m. Note that for $k_{max} = 3$ the critical disorder parameter is $m^c_3 \approx 1.918$. Since the minimum value of the derivative $d\sigma/d\varepsilon$ Eq. (3·5) is positive in the high disorder phase, the avalanche size distribution $P(\Delta)$ behaves as in simple fiber bundles when the loading process was stopped at a deformation ε_m before the critical point of macroscopic failure.[9] It follows that for $m < m^c_{k_{max}}$ the size distribution of bursts takes the form $P(\Delta) \sim \Delta^{-\tau} e^{-[a(\varepsilon_m)-1-\ln a(\varepsilon_m)]\Delta}$, i.e. the power law regime of exponent $\tau = 9/4$ is followed by an exponential cutoff, where in our case ε_m is the position of the inflexion point of the constitutive curve. Since in the high disorder phase of the model only relatively small avalanches pop up away from the phase boundary, this phase is called POP phase.[3]

Figure 8(a) presents the size distribution of slip avalanches $P(\Delta)$ obtained by computer simulations for $k_{max} = 7$ at different m values in the range $m \leq m^c_7$. A high quality power law behavior is obtained with a diverging cutoff as approaching the critical point $m \to m^c_7$ in agreement with the above derivation. It follows from the above equations that the cutoff avalanche size Δ_0 of $P(\Delta)$ has a power law divergence as a function of the distance from the corresponding critical point $m^c_{k_{max}}$, i.e. $\Delta_0 \sim (m^c_{k_{max}} - m)^{-\nu}$ is obtained with the exponent $\nu = 1/2$.

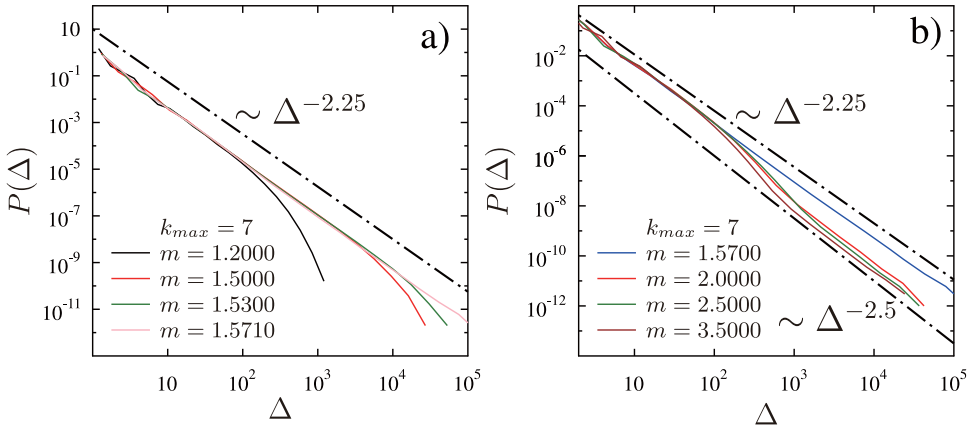

Fig. 8. (a) Size distribution of slip avalanches in the POP phase of the model for several values of m at the fixed $k_{max} = 7$. As m approaches $m_7^c \approx 1.5712$ the cutoff avalanche size diverges. (b) Comparison of avalanche size distributions in the POP and $SNAP$ phases. Excellent agreement is obtained with the analytic predictions.

The parameter regime above the $m^c_{k_{max}}$ curve of Fig. 7 defines the low disorder phase of the model where the constitutive curve can have local maxima along the plateau regime (see also Fig. 6(b)). At a given value of k_{max} the number of maxima of $\sigma(\varepsilon)$ is one if the value of m falls in the interval $m^c_{k_{max}} < m < e$. Under stress controlled loading a macroscopic avalanche appears resulting in a horizontal jump when the maximum of $\sigma(\varepsilon)$ is reached. Consequently, this phase of the model is called $SNAP$ phase.[3] Starting from Eq. (3·5) it can be shown that at very low disorder $m > e$, i.e. when the probability density p of slip thresholds is very narrow, the constitutive curve has a local maximum already at $k_{max} = 1$ and further maxima occur with decreasing height accompanied by a similar oscillating behavior of $a(\varepsilon)$ as k_{max} increases. In the $SNAP$ phase the distribution of avalanche sizes $P(\Delta)$ is determined by the first maximum of $\sigma(\varepsilon)$ which has a quadratic shape. Consequently, similarly to the case of simple fiber bundles, $P(\Delta)$ has a power law functional form $P(\Delta) \sim \Delta^{-\tau}$ without cutoff regime but with an exponent $\tau = 5/2$ higher than in the POP phase.[9)–11)] Burst size distributions of the POP and $SNAP$ phases are compared in Fig. 8(b), where nice agreement can be observed with the analytic predictions.

Our analytical calculations and computer simulations showed that disorder plays a very important role in the avalanches of restructuring events. Varying the amount of disorder and the number of allowed slips the mean field system undergoes a phase transition from the phase where only small avalanches pop up to another one where macroscopic avalanches snap the entire system.

§4. Discussion

Disorder has a strong effect on the fracture process of heterogeneous materials both on the macro and micro scales. Under a slowly increasing external load, due

to the quenched structural disorder of materials, a stochastic sequence of crack nucleation, growth, and arrest arises which results in the emergence of crackling noise. In spite of the smooth macroscopic constitutive behavior, on the microscale fracture proceeds in a discrete sequence of events, i.e. bursts which emit acoustic noise. The investigation of crackling noise can provide very valuable information on the microscopic dynamics of fracture (non-destructive testing) and it can also be used to forecast the imminent macroscopic failure of the system.

In the present paper we investigated the effect of the amount of disorder on the properties of crackling noise emerging in heterogeneous materials under a slow external driving. In order to gain information about the relevance of spatial correlations in the emergence of crackling, we compared two different types of fracture problems: first we considered the propagation of a single crack in a specimen which is subject to a three-point bending load, then we studied the noisy rearrangements of a bundle of fibers under a slowly increasing uniaxial load.

Computer simulations showed that the crack emerging under three-point bending conditions proceeds in correlated jumps with widely different sizes. When the crack penetrates a weak region it proceeds faster, however, reaching a stiffer zone it gets pinned. As the crack advances larger and larger stress concentration arises at the crack tip which drives the crack advancement. Our calculations revealed that decreasing the amount of disorder the crack tip makes larger jumps so that the average burst/jump size increases. The distribution of burst sizes exhibits a power law decay for small bursts while it has a rapidly decreasing exponential shape for the large ones. The value of the exponent of the power law regime is in a reasonable agreement with the experimental findings of Ref. 19). The most important outcome of our work is that varying the amount of disorder the functional form of the jump distribution remains the same and we proposed a scaling form of the size distribution using the average burst size as a scale variable.

As a second step we analyzed avalanches of restructuring events in a bundle of fibers which respond to an increasing load by stick-slip mechanism. The main difference of the two systems investigated is that in the first case bursts are composed of spatially correlated breaking sequences which localize at the crack tip, while in the second one the system is of mean field type and spatial correlations do not occur. Our analytical calculations and computer simulations showed that varying the amount of disorder and the total number of allowed slips the system undergoes a phase transition: at high disorder only small avalanches pop up in the system while at low disorder avalanches comparable to the system size may occur. When approaching the phase boundary from the high disorder phase the characteristic avalanche size exhibits a power law divergence resembling to second order phase transitions.

In heterogeneous materials subject to external load local breakings occur as the result of the competition of two mechanisms: breaking due to local weaknesses of the material (quenched disorder) and breaking due to local overloads (stress concentration) in the vicinity of failed regions. Our study revealed that when the stress concentration dominates the process, the amount of disorder only changes the scale of crackling noise but the characteristic probability distributions retain their functional form. In the mean field model of stick-slip avalanches where disorder dominates the

stick-slip sequences, a phase transition is obtained when changing the amount of disorder. Recently, we have carried out a mean field study of cracking under three-point bending conditions, where the interface between two rigid blocks was discretized in terms fibers.[22] Analytic calculations and computer simulations revealed a power law distribution of burst sizes with a crossover in the burst exponent with decreasing disorder, which is consistent with the above arguments.

Acknowledgements

F. Kun acknowledges the financial support of Hungarian Academy of Sciences (Janos Bolyai program) and the support of the MTA-JSPS program. This work was partially supported by the Yukawa International Program for Quark-Hadron Sciences (YIPQS).

References

1) M. Alava, P. K. V. Nukala and S. Zapperi, Adv. Phys. **55** (2006), 349.
2) J. P. Sethna, K. A. Dahmen and C. R. Meyers, Nature **410** (2001), 242.
3) F.-J. Pérez-Reche, L. Truskinovsky and G. Zanzotto, Phys. Rev. Lett. **101** (2008), 230601.
4) K. A. Dahmen, Y. Ben-Zion and J. T. Uhl, Phys. Rev. Lett. **102** (2009), 175501.
5) J. P. Sethna, K. A. Dahmen, S. Kartha, B. W. Roberts and J. L. Shore, Phys. Rev. Lett. **70** (1993), 3347.
6) G. Durin and S. Zapperi, Phys. Rev. Lett. **84** (2000), 4705.
7) M.-C. Miguel, A. Vespignani, S. Zapperi, J. Weiss and J.-R. Grasso, Nature **410** (2001), 667.
8) J. Davidsen, S. Stanchits and G. Dresen, Phys. Rev. Lett. **98** (2007), 125502.
9) M. Kloster, A. Hansen and P. C. Hemmer, Phys. Rev. E **56** (1997), 2615.
10) S. Pradhan, A. Hansen and P. C. Hemmer, Phys. Rev. Lett. **95** (2005), 125501.
11) R. C. Hidalgo, K. Kovács, I. Pagonabarraga and F. Kun, Europhys. Lett. **81** (2008), 54005.
12) N. Yoshioka, F. Kun and N. Ito, Phys. Rev. Lett. **101** (2008), 145502.
13) F. Kun, S. Zapperi and H. J. Herrmann, Eur. Phys. J. B **17** (2000), 269.
14) F. Kun, H. A. Carmona, J. S. Andrade Jr. and H. J. Herrmann, Phys. Rev. Lett. **100** (2008), 094301.
15) B. Behera, F. Kun, S. McNamara and H. J. Herrmann, J. of Phys.: Cond. Mat. **17** (2005), S2439.
16) F. Kun and H. J. Herrmann, Phys. Rev. E **59** (1999), 2623.
17) F. Kun and H. J. Herrmann, Comput. Methods Appl. Mech. Eng. **138** (1996), 3.
18) F. Kun and H. J. Herrmann, Int. J. Mod. Phys. C **7** (1996), 837.
19) F. Kun, Gy. B. Lenkey, N. Takács and D. L. Beke, Phys. Rev. Lett. **93** (2004), 227204.
20) Z. Halász and F. Kun, Phys. Rev. E **80** (2009), 027102.
21) R. Burridge and L. Knopoff, Bull. Seis. Soc. Amer. **57** (1967), 341.
22) F. Kun and S. Nagy, Phys. Rev. E **77** (2008), 016608.